Milberg et al., https://doi.org/10.1083/jcb.201612126

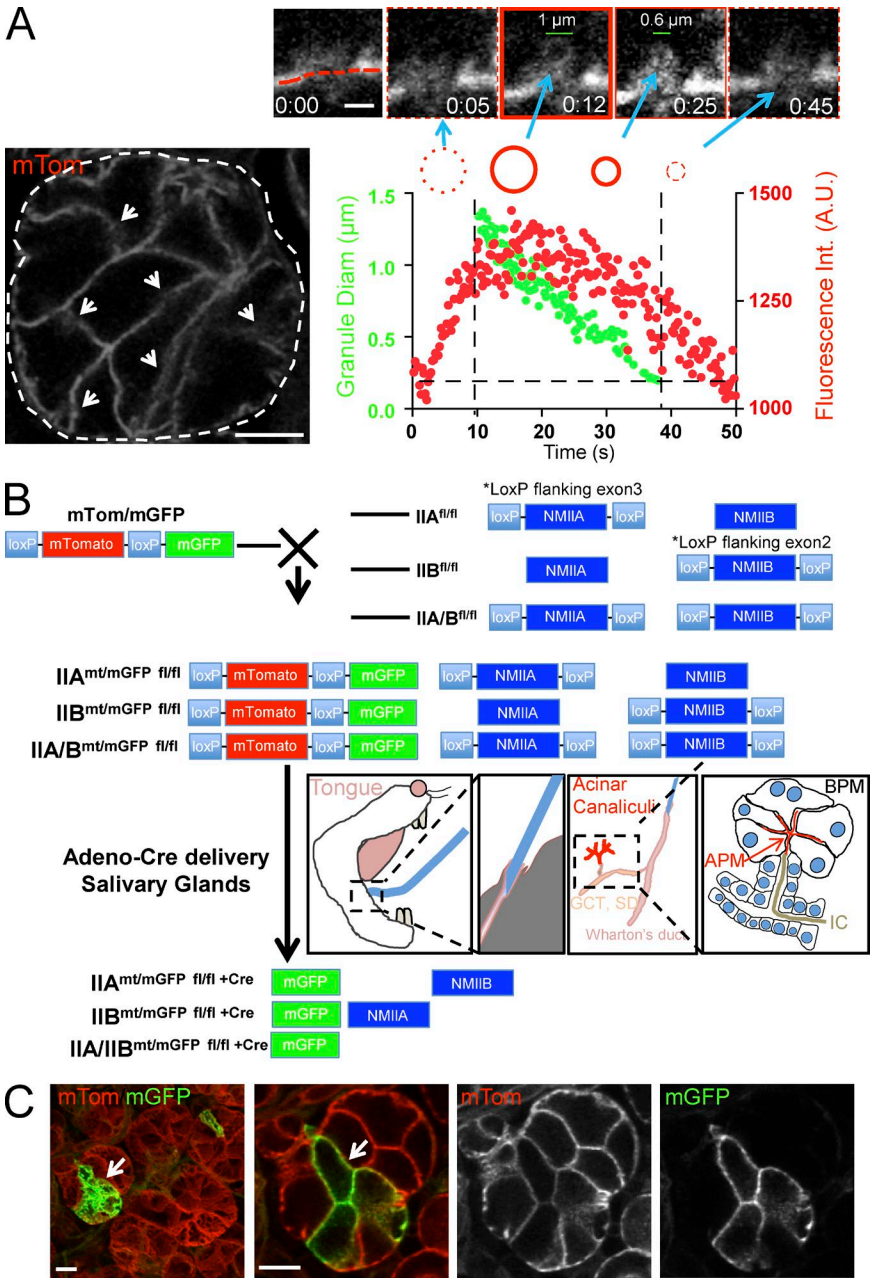

Figure S1. **Membrane/Cre reporter mice and generation of floxed NMII mice with a Cre reporter.** (A) mT/mGFP mice were anesthetized, and the SGs were surgically exposed. 0.03 mg/kg ISO was injected SC, and the glands were imaged by confocal microscopy. (Left) A single acinus (dashed line) and the APM (arrows). Bar, 20 µm. (Insets) A close up of the APM (red dashed line) and the kinetics of the integration of a secretory granule (blue arrows). Bar, 1 µm. (Right) The fluorescence intensity (Int.; red dots) and the diameter (Diam; green dots) of each granule were measured, as described in Materials and methods, and reported as a function of time. The graph shows representative data from the granule in the insets. Note that, in the first 10 s from the detection of the mT fluorescence in the membranes of the granules, it is not possible to clearly define their diameter (compare time 0:05 and 0:12). (B) Mice in which loxP sites flank Exon 3 and Exon 2 of the NMIIA ($IIA^{fl/fl}$) and NMIIB ($IIB^{fl/fl}$) genes, respectively, were crossed with mice expressing the Cre recombinase (Cre) reporter mT/mGFP, in which a plasma membrane–targeted peptide tagged with the tandem-tomato protein (mT) is replaced by a similar peptide tagged with GFP (mGFP) upon Cre expression. In addition, $IIA^{fl/fl}$ and $IIB^{fl/fl}$ mice were first crossed to generate an $IIA/IIB^{fl/fl}$ strain, which was then crossed with the mT/mGFP mouse. An adenovirus engineered to express Cre (Ade-Cre) was delivered to the submandibular SGs by retroinjection into the salivary ducts of anesthetized mice as described in Materials and methods. BPM, basolateral plasma membrane; GCT, granular convoluted tubules; IC, intercalated duct; SD, striated duct. (C) mT/mGFP mice were injected with Ade-Cre (10^9 particles per gland). After 14 d, the mice were anesthetized, and the SGs were exposed and imaged by confocal microscopy. (Left) Maximal projection of a z stack of acini located within the first 50 µm from the gland's surface. The Cre-expressing cells can be easily identified by the expression of the mGFP reporter (arrows). (Right) A single optical section of two adjacent acini. Bars, 20 µm.

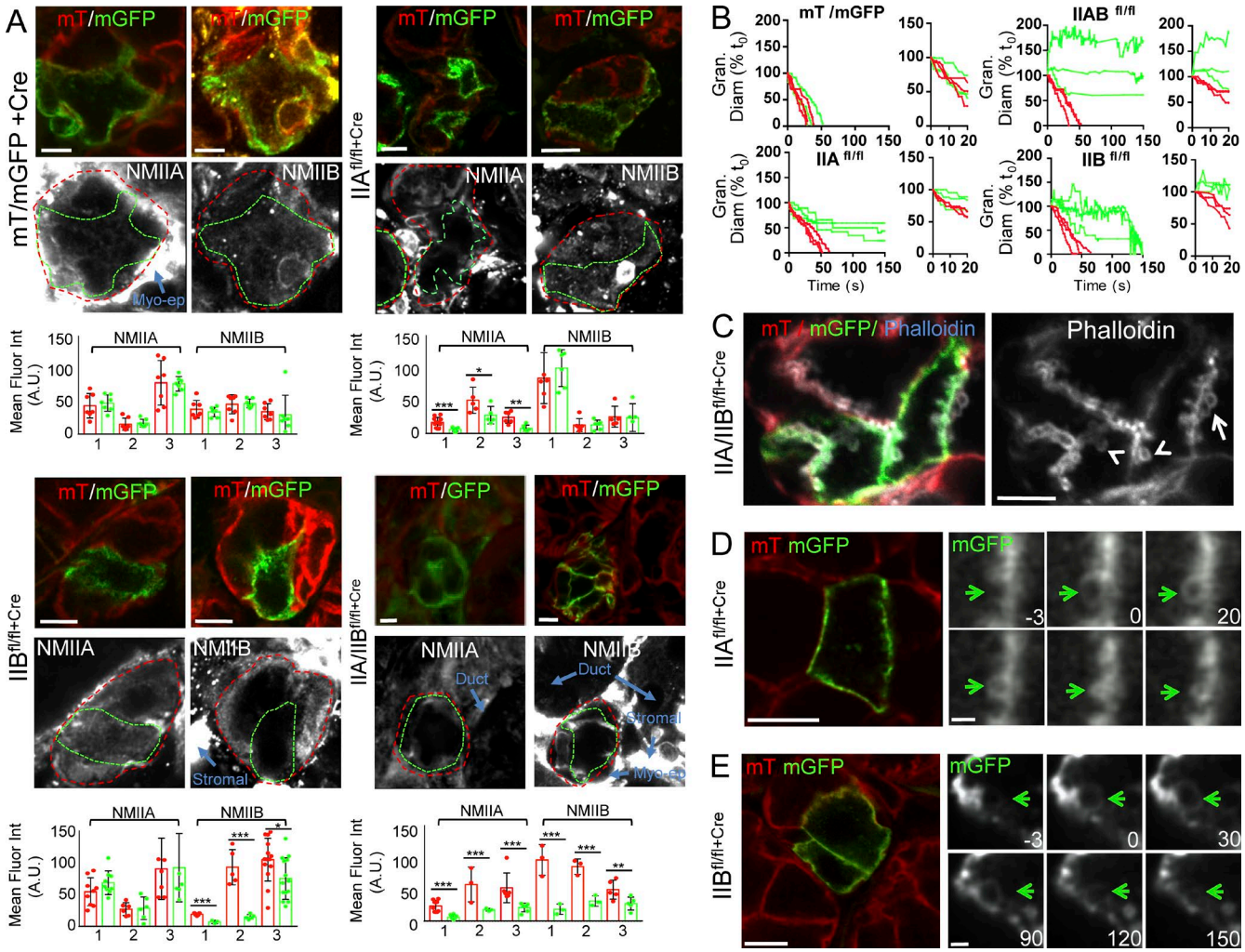

Figure S2. **Characterization of IIA$^{fl/fl}$, IIB$^{fl/f}$, and IIAB$^{fl/f}$ mice.** (A–E) 10^9 particles of Ade-Cre were retroinjected into the submandibular SGs of mT/mGFP, IIA$^{fl/fl}$, IIB$^{fl/fl}$, and IIAIIB$^{fl/fl}$ mice, as described in Fig. S1. After 14 d, the animals were either euthanized by cardiac fixation and the SGs were excised and processed for indirect immunofluorescence (A) or anesthetized and the SGs were imaged by confocal time-lapse microscopy (B–E). (A) Immunofluorescence labeling (top) and quantification (bottom) of NMIIA and NMIIB in SG acini from mT/mGFP, IIA$^{fl/fl}$, IIB$^{fl/fl}$, and IIAIIB$^{fl/fl}$ mice expressing Cre. (Top) mT (red) and mGFP (green) fluorescence. (Middle) Labeling for either NMIIA or NMIIB (gray). Cre-expressing cells are highlighted with green dashed lines, acini are delineated with red dashed lines, and the blue arrow highlight ducts and myoepithelial (Myo-ep) cells that express almost no and very high levels of NMII. Bars, 10 µm. (Bottom) Mean fluorescence intensity (Fluor Int) of NMIIA and NMIIB in Cre-positive (green) and Cre-negative (red) cells from three (labeled 1, 2, and 3) mT/mGFP (n = 21 cells), IIA/IIB$^{fl/fl}$ (n = 19 cells), IIA$^{fl/fl}$ (n = 22 cells), and IIB$^{fl/fl}$ (n = 22 cells) mice. Error bars represent SD. *, P < 0.05; **, P < 0.01; ***, P < 0.0001; Student's t test. (B) Change over time in diameter (Diam.) of individual secretory granules (Gran.) during integration in Cre-positive (green) and Cre-negative (red) cells. (Insets) Granule diameters in the first 20 s of integration. For each graph, three representative granules were chosen for Cre-positive and Cre-negative cells, respectively. (C) SGs of IIA/IIB$^{fl/fl}$ mice were labeled with Alexa Fluor 647 phalloidin. F-actin is recruited onto the secretory granules even in absence of the NMII isoforms. Arrowheads point to granules in Cre-expressing cells, and the arrow points to a granule in a cell not expressing Cre. Bar, 20 µm. (D and E) Low magnification of the Cre-transfected cell expressing mGFP in IIA$^{fl/fl}$ (D, left) and IIB$^{fl/fl}$ (E, left). Bars, 20 µm. Time-lapse series of the integration of the secretory granules (green arrows; right) with the APM scale. Bars, 2 µm. Time 0 represents the moment in which the limiting membranes of the granules were detected.

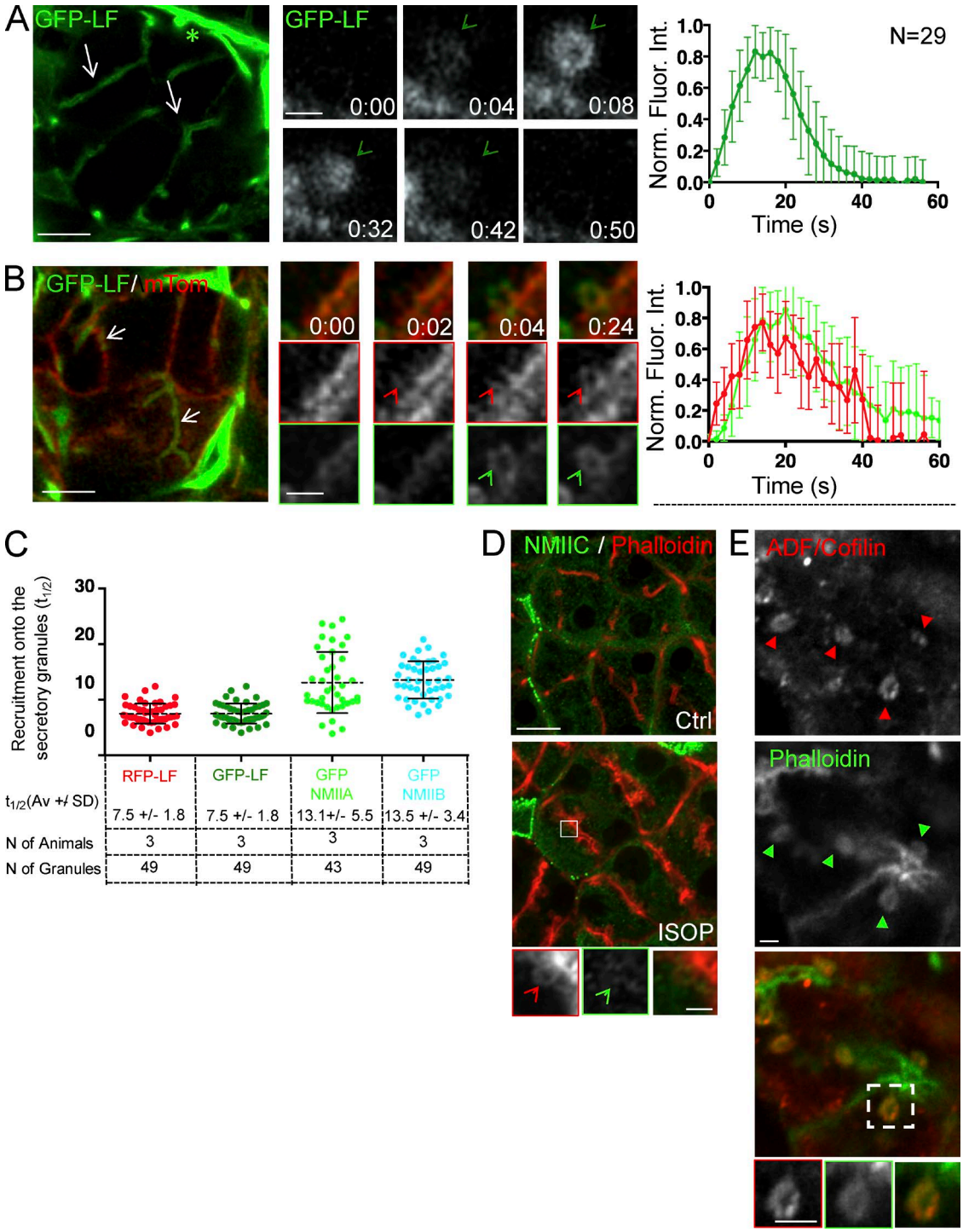

Figure S3. **Kinetics of recruitment of the actin cytoskeleton onto the secretory granules.** (A–C) ISMic of salivary acini in mice expressing GFP-LF either alone (A) or in combination with mTomato (mTom; B). Left panels show low magnifications of individual acini and the localization of GFP-LF at the APM (arrows; bars, 20 µm), whereas middle panels show time-lapse imaging of their recruitment onto the secretory granules (arrowheads; bars, 1 µm). The asterisk represents a myoepithelial cell. In B, mT (red arrowheads) appears on the secretory granules before GFP-LF (green arrowheads). (Right) The graphs show the kinetics of appearance onto the secretory granules of GFP-LF, either alone or with respect to the mT probe. The fluorescent intensity (Fluor. Int.) around the granules was measured during their integration, normalized (Norm.), and reported as a function of time, as described in Materials and methods. The curve in A represents the mean ± SD from one of three animals (N = number of granules), whereas the curve in B is from one representative granule (5–10 granules per animal, total of three animals). (C) The $t_{1/2}$ of the recruitment of RFP-LF (red), GFP-LF (dark green), GFP-NMIIA (light green), and GFP-NMIIB (cyan) was calculated as described in Materials and methods. Mean ± SD is shown. The number of animals and total number of granules scored are reported in the table below the graph. (D and E) Wild-type mice were either left untreated (D, top) or injected with 0.03 mg/kg ISOP (D, bottom; and E), and the SGs were processed for immunofluorescence. (D) The glands were stained with antibodies against NMIIC (green) and Alexa Fluor 594–phallodin (red). Bar, 20 µm. NMIIC is not recruited onto the fused secretory granules (insets, arrowheads; bar, 2 µm). Ctrl, control. (E) The glands were stained with antibodies against ADF-Cofilin (red) and Alexa Fluor 488–phallodin (green). ADF/cofilin is recruited onto the fused secretory granules (arrowheads and insets). Bars, 2 µm.

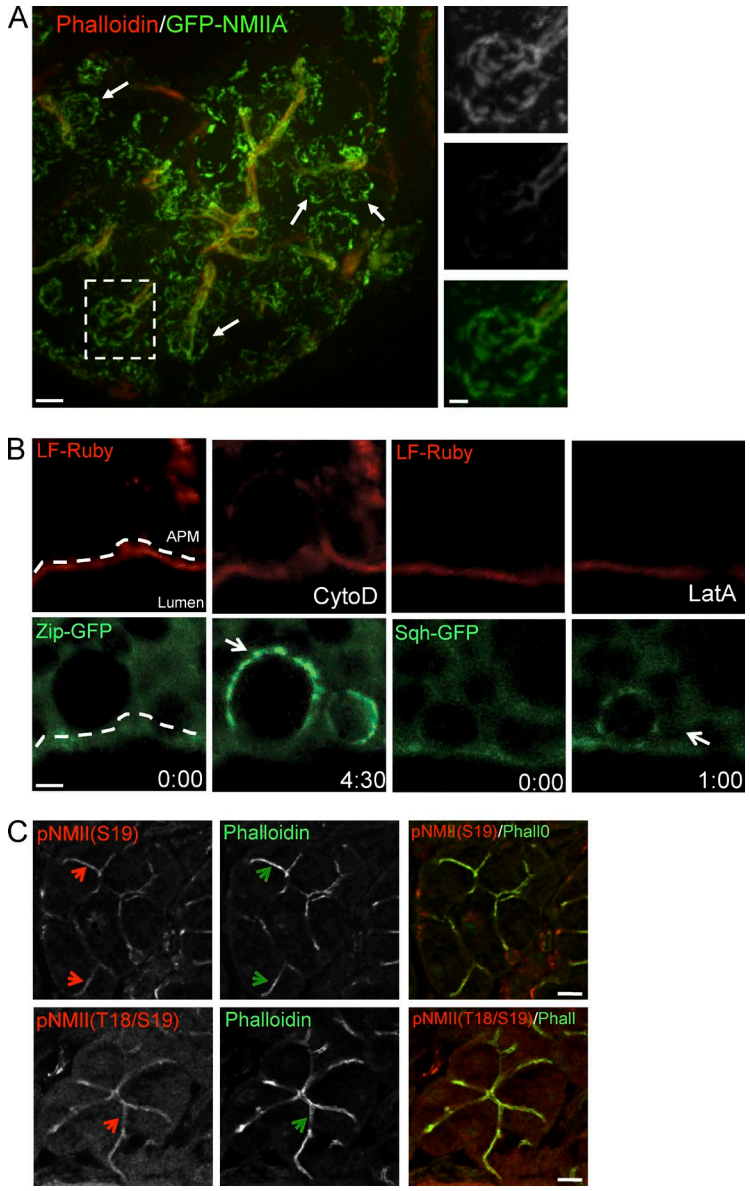

Figure S4. **NMII localizes to secretory granules despite inhibition of F-actin and phosphorylation of NMII light-chain kinase under resting conditions.** (A) Mice expressing GFP-NMIIA were exposed to 10 µM LatA for 20 min and injected SC with 0.03 mg/kg ISOP, as described in Materials and methods. The SGs were explanted, processed for immunofluorescence, and labeled with Alexa Fluor phalloidin. Arrows point to enlarged granules. The series of small panels shows high magnification of an individual enlarged granule boxed on the left. Bars, 2 µm. (B) Secreting *Drosophila* SGs expressing LF-Ruby and either Zip-GFP (left) or Sqh-GFP (right) were treated with CytD (left) or LatA (right) and imaged in time-lapse modality as described by Tran et al. (2015). Dashed lines delineate the APM, and arrows point to enlarged granules coated with Zip-GFP. Bar, 5 µm. (C) The SGs of wild-type mice were processed for immunofluorescence and stained with antibodies against the phosphorylated forms of NMII (red) and Alexa Fluor 488–phallodin (green). Mono- and diphosphorylated NMII RLCs are localized at the APM (arrowheads). Bars, 20 µm.

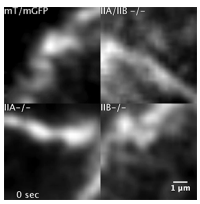

Video 1. **Integration of secretory granules into the APM in various mice, as visualized by time-lapse intravital confocal microscopy.** Excitation is at 488 nm. The video is related to Fig. 1. Membranes are highlighted by the mGFP probe expressed upon Cre injection. One frame was acquired every second, and the video is displayed at 10 frames per second.

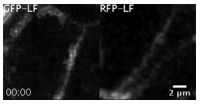

Video 2. **Recruitment of GFP-LF and RFP-LF onto the secretory granules fused with the APM, as visualized by time-lapse intravital confocal microscopy.** Excitation is at 488 and 561 nm. The video is related to Figs. 2 and S3. One frame was acquired every second, and the video is displayed at 10 frames per second.

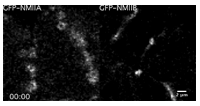

Video 3. **Recruitment of GFP-NMIIA and GFP-NMIIB onto the secretory granules fused with the APM, as visualized by time-lapse intravital confocal microscopy.** Excitation is at 488 nm. The video is related to Figs. 2 and S3. One frame was acquired every second, and the video is displayed at 10 frames per second.

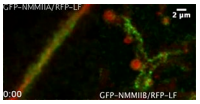

Video 4. **Recruitment of NMIIA onto secretory granules fused at the APM with respect to F-actin.** Time-lapse images were acquired in mice expressing RFP-LF (red) and either GFP-NMIIA or GFP-NMIIB (green) by time-lapse intravital confocal microscopy. Excitation is at 488 and 561 nm. One frame was acquired every second, and the video is displayed at 10 frames per second.

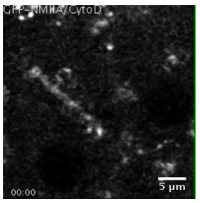

Video 5. **Recruitment of GFP-NMIIA onto the secretory granules fused with the plasma membrane and treated with 10 µM CytoD.** Time-lapse images were acquired in mice expressing GFP-NMIIA by time-lapse intravital confocal microscopy. Excitation is at 488 nm. One frame was acquired every second, and the video is displayed at 10 frames per second.

Reference

Tran, D.T., A. Masedunskas, R. Weigert, and K.G. Ten Hagen. 2015. Arp2/3-mediated F-actin formation controls regulated exocytosis in vivo. *Nat. Commun.* 6:10098. http://dx.doi.org/10.1038/ncomms10098